High-resolution terrestrial climate, bioclimate and vegetation for the last 120,000 years

Robert M. Beyer[1,*], Mario Krapp[1], Andrea Manica[1]

August 14, 2019

1. Department of Zoology, University of Cambridge, Downing Street, Cambridge CB2 3EJ, United Kingdom
* Corresponding author: Robert M. Beyer (rb792@cam.ac.uk)

Abstract

The variability of climate has profoundly impacted a wide range of macroecological processes in the Late Quaternary. Our understanding of these has greatly benefited from palaeoclimate simulations, however, high-quality reconstructions of ecologically relevant climatic variables have been limited to a few selected time periods, thus impeding continuous-time analyses. Here, we present a 0.5° resolution bias-corrected dataset of global monthly temperature, precipitation, cloud cover, relative humidity and wind speed, 17 bioclimatic variables, net primary productivity and biomes covering the last 120,000 years at a temporal resolution of 1,000–2,000 years. The data are derived by combining medium-resolution HadCM3 climate simulations of the last 120,000 years with high-resolution HadAM3H simulations of the last 21,000 years and present-day observational data. Our approach allows for the temporal variability of small scale features while ensuring consistency with observed climate. The data show a good agreement with empirical reconstructions of temperature, precipitation and vegetation for the mid-Holocene, the Last Glacial Maximum and the Last Interglacial, performing equally well as existing high-resolution snapshot simulations of these time periods.

Background & Summary

Global climate in the Late Quaternary has played a major role in the formation of a wide range of macroecological patterns. Reconstructing climatic conditions has been crucial in advancing our understanding of the spatial and temporal dynamics of these processes, ranging from the distribution of species ranges [16, 22] and extinctions [13], to early human expansions [23] and population genetics [6].

Climate models can provide the spatial coverage that localised empirical reconstructions are lacking; however, currently available simulation data for the

Late Pleistocene and the Holocene suffer from one of two drawbacks that limit their use for ecological applications. On the one hand, a number of equilibrium and transient simulations, from general circulation models (e.g. HadCM3 [20]) or earth system models of intermediate complexity (e.g. LOVECLIM [23]), provide reconstructions at a high temporal resolution, however, the relatively low spatial resolution of the simulated data, and significant biases when compared to empirical observations, make additional curating of model outputs necessary, in order to generate ecologically meaningful data. On the other hand, several high-resolution and bias-corrected palaeoclimate datasets provide climatic variables in great spatial detail, but their temporal coverage of the Late Pleistocene and the Holocene is usually limited to a few snapshots of key time periods. A number of these datasets have been made available in readily accessible formats since the mid 2000s, and have since been used extensively in ecological applications: the ecoClimate database [12] provides data for the Mid-Holocene (∼6,000 BP) and the Last Glacial Maximum (∼21,000 BP); WorldClim [9] contains an additional reconstruction of the Last Interglacial Period (∼130,000 BP); paleoClim [4] covers the last 21,000 years.

Here, we fill the gap between these two categories of available data, by deriving a high-resolution (0.5°) bias-corrected time series of global terrestrial climate and vegetation data covering the last 120,000 years. Gridded reconstructions (Table 1) are available at 2,000 year time steps between 120,000 and 22,000 BP, and 1,000 year time steps between 21,000 BP and the present. Like previous datasets available for specific time periods, our data include monthly temperature and precipitation, and 17 bioclimatic variables, which have been used extensively in species distribution models (e.g. [18]). We also provide monthly cloudiness, relative humidity and wind speed (which can be used to derive various measures of apparent temperature), as well as reconstructions of global biomes, leaf area index and net primary productivity.

Methods

Monthly climatic variables

Our dataset is based on simulations of monthly mean temperature (°C), precipitation (mm year^{-1}), cloudiness (%), relative humidity (%) and wind speed (m s^{-1}) from the HadCM3 general circulation model [25], covering the last 120,000 years in 72 snapshots (2,000 year time steps between 120,000 BP and 22,000 BP; 1,000 year time steps between 22,000 BP and the present) at a 3.75°×2.5° grid resolution. We denote these data by

$$\begin{gathered} T_{\text{HadCM3}}(m,t),\ P_{\text{HadCM3}}(m,t),\ C_{\text{HadCM3}}(m,t), \\ H_{\text{HadCM3}}(m,t),\ W_{\text{HadCM3}}(m,t), \end{gathered} \tag{1}$$

where $m = 1, \ldots, 12$ represents a given month, and $t \in T_{120\text{k}}$ represents a given one of the 72 points in time, denoted $T_{120\text{k}}$, for which simulations are available.

We downscaled and bias-corrected these data in two stages (Fig. 1). Both use variations of the Delta Method [14], under which a high-resolution, bias-corrected reconstruction of climate at some time t is obtained by applying the difference between lower-resolution present-day simulated and high-resolution present-day observed climate – the correction term – to the simulated climate at time t. The Delta Method has been used to downscale and bias-correct palaeoclimate simulations before (e.g. for the WorldClim database [9]), and, despite its conceptual simplicity, has been shown to outperform alternative methods commonly used for bias-correction and downscaling [3].

Downscaling to $\sim 1^\circ$ resolution

A key limitation of the Delta Method is that it assumes the present correction term to be representative of past correction terms. This assumption is substantially relaxed in the Dynamic Delta Method [11] used in the first stage of our approach to downscale the above data (1) to a $\sim 1^\circ$ resolution. This involves the use of a set of high-resolution climate simulations that were run for a smaller but climatically diverse subset of T_{120k}. Simulations at this resolution are highly computationally expensive, and therefore running substantially larger sets of simulations is not feasible; however, these selected data can be very effectively used to generate a suitable (time-dependent) correction term for each $t \in T_{120k}$. In this way, we are able to increase the resolution of the original climate simulations by a factor of ~ 9, whilst simultaneously allowing for the temporal variability of the correction term. In the following, we detail the approach.

We used high-resolution simulations of the same variables as in (1) from the HadAM3H model [25], available for the last 21,000 years in 9 snapshots (2,000 year time steps between 12,000 BP and 6,000 BP; 3,000 year time steps otherwise) at a $1.25^\circ \times 0.83^\circ$ resolution. We denote these by

$$T_{\mathrm{HadAM3H}}(m,t),\ P_{\mathrm{HadAM3H}}(m,t),\ C_{\mathrm{HadAM3H}}(m,t),$$
$$H_{\mathrm{HadAM3H}}(t),\ W_{\mathrm{HadAM3H}}(m,t),$$

respectively, where $t \in T_{21k}$, and T_{21k} represents the 9 points in time for which HadAM3H simulations are available. These data were used to downscale the relevant HadCM3 variables (1) to a $1.25^\circ \times 0.83^\circ$ resolution by means of the Dynamic Delta Method [11], yielding

$$X_{\sim 1^\circ}(t) := X^{\boxplus}_{\mathrm{HadCM3}}(t) + \underbrace{X_{\mathrm{HadAM3H}}(\hat{t}) - X^{\boxplus}_{\mathrm{HadCM3}}(\hat{t})}_{\text{time-variable correction term}}, \tag{2}$$

for $X \in \{T, P, C, H, W\}$. We discuss the choice of an additive approach for all climatic variables in detail later on. The $\boxplus$-notation indicates that the coarser-resolution data was interpolated to the grid of the higher-resolution data, for which we used an Akima cubic Hermite interpolant [1], which (unlike the bilinear interpolation) is continuously differentiable but (unlike the bicubic interpolation) avoids overshoots. Crucially, the time $\hat{t} \in T_{21k}$ in (2) is chosen

as the time at which climate was, in a sense specified below, close to that at time $t \in T_{120k}$. Thus, in contrast to the classical Delta Method (for which $\hat{t} = 0$ for all t), the approach in (2a) does not assume the resolution correction term, $X_{\mathrm{HadAM3H}}(\hat{t}) - X^{\boxplus}_{\mathrm{HadCM3}}(\hat{t})$, to be constant over time. Instead, the high-resolution heterogeneities that are applied to the medium-resolution HadCM3 data are chosen from the range of patterns simulated for the last 21,000 years. The strength of the approach lies in the fact that the last 21,000 years account for a substantial portion of the range of climatic conditions present during the whole Late Quaternary. Following [11], we used global CO_2, a key indicator of the global climatic state, as the metric according to which $\hat{t}$ is chosen; i.e., among the times for which HadAM3H simulations are available, $\hat{t}$ is the time at which global CO_2 was closest to the respective value at the time of interest, t.

Bias-correction and downscaling to 0.5° resolution

In the second stage of our approach, we applied the classical Delta Method to the previously downscaled data, using 0.5° resolution observed present-day (1960–1990 average) terrestrial monthly temperature, precipitation, cloudiness, relative humidity and wind speed [15], denoted

$$T_{\mathrm{obs}}(m,0),\ P_{\mathrm{obs}}(m,0),\ C_{\mathrm{obs}}(m,0),\ H_{\mathrm{obs}}(m,0),\ W_{\mathrm{obs}}(m,0).$$

We extrapolated these data to current non-land grid cells using an inverse distance weighting approach in order to use the Delta Method at times of lower sea level. The resulting data was used to bias-correct and further downscale the $\sim 1°$ data (2) to a 0.5° grid resolution analogously as in (2):

$$X'_{0.5°}(m,t) := X^{\boxplus}_{\sim 1°}(m,t) + \underbrace{X_{\mathrm{obs}}(m,0) - X^{\boxplus}_{\sim 1°}(m,0)}_{\text{correction term}}, \tag{3}$$

where $X \in \{T, P, C, H, W\}$.

The additive approach used here does not ensure that the derived precipitation, relative humidity, cloudiness and wind speed are nonnegative and that relative humidity, cloudiness do not exceed 100% across all points in time and space. Thus, we cap values at the appropriate boundaries, and obtain

$$\begin{aligned}
T_{0.5°}(m,t) &:= T'_{0.5°}(m,t),\\
P_{0.5°}(m,t) &:= \max(0, P'_{0.5°}(m,t)),\\
C_{0.5°}(m,t) &:= \min(100\%, \max(0\%, C'_{0.5°}(m,t))),\\
H_{0.5°}(m,t) &:= \min(100\%, \max(0\%, H'_{0.5°}(m,t))),\\
W_{0.5°}(m,t) &:= \max(0, W'_{0.5°}(m,t)).
\end{aligned} \tag{4a}$$

In principle, capping values, where necessary, can be circumvented by suitably transforming the relevant variable first, then applying the additive Delta Method, and back-transforming the result. In the case of precipitation, for instance, a log-transformation is sometimes used, which is mathematically equiv-

alent to a multiplicative Delta Method, in which low-resolution past simulated data gets multiplied by the relative difference between high- and low-resolution data at present-day [14]. For example, instead of (3), we would have $P_{0.5^\circ}(m,t) := P^{\boxplus}_{\sim 1^\circ}(m,t) \cdot \frac{P_{\mathrm{obs}}(m,0)}{P^{\boxplus}_{\sim 1^\circ}(m,0)}$. Whilst this approach does ensure non-negative values, it has three important drawbacks. First, if present-day observed precipitation in a certain month and grid cell is zero, $P_{\mathrm{obs}}(m,0) = 0$, then $P_{0.5^\circ}(m,t) = 0$ for all points in time, t, irrespective of the simulated climate change signal, thus making it impossible for current extreme desert areas to be wetter in the past. Second, if present-day simulated precipitation in a grid cell is very low (or identical to zero), $P^{\boxplus}_{\sim 1^\circ}(m,0) \approx 0$, then $P_{0.5^\circ}(m,t)$ can increase beyond all bounds. Very arid locations are particularly prone to this effect, which can generate highly improbable precipitation patterns for the past. In our scenario of generating global maps for a total of 864 individual months, this lack of robustness of the multiplicative Delta Method would be difficult to handle. Third, the multiplicative Delta Method is not self-consistent, in that applying it to the sum of simulated monthly precipitation does not generate the same result as applying it to simulated monthly precipitation and taking the sum of these values. The natural equivalent of the log-transformation for precipitation is the logit-transformation for cloudiness and relative humidity, however, this approach suffers from the same drawbacks.

Minimum and maximum annual temperature

Diurnal temperature data are not included in the available HadCM3 and HadAM3H simulation outputs. We therefore used the following approach to estimate the minimum and maximum annual temperature. Based on the monthly HadCM3 and HadAM3H temperature data, we created maps of the mean temperature of the coldest and the warmest month. In the same way as described above, we used these data to reconstruct the mean temperature of the coldest and warmest month at a $1.25^\circ \times 0.83^\circ$ resolution by means of the Dynamic Delta Method, yielding

$$T^{\text{coldest month}}_{\sim 1^\circ}(t) \quad \text{and} \quad T^{\text{warmest month}}_{\sim 1^\circ}(t),$$

where $t \in T_{120k}$. We then used 0.5° resolution maps of observed present-day minimum and maximum annual temperature [7],

$$T^{\min}_{\mathrm{obs}}(0) \quad \text{and} \quad T^{\max}_{\mathrm{obs}}(0),$$

to estimate past minimum and maximum annual temperature as

$$\begin{aligned} T^{\min}_{0.5^\circ}(t) &:= T^{\text{coldest month},\boxplus}_{\sim 1^\circ}(t) + T^{\min}_{\mathrm{obs}}(0) - T^{\text{coldest month},\boxplus}_{\sim 1^\circ}(0) \\ T^{\max}_{0.5^\circ}(t) &:= T^{\text{warmest month},\boxplus}_{\sim 1^\circ}(t) + T^{\min}_{\mathrm{obs}}(0) - T^{\text{warmest month},\boxplus}_{\sim 1^\circ}(0) \end{aligned} \tag{4b}$$

respectively. This assumes that the difference between past and present mean temperature of the coldest (warmest) month is similar to the difference between the past and present minimum (maximum) annual temperature.

Land configuration

We used a reconstruction of mean global sea level [21] and a global elevation and bathymetry map [5], interpolated to a 0.5° resolution grid, to create land configuration maps for the last 120,000 years. Maps of terrestrial climate were obtained by cropping the global data in (4a–b) to the derived land masks. Values in non-land grid cells were set to missing values, except in the case of below-sea-level inland grid cells, such as the Aral, Caspian and Dead sea.

Bioclimatic data, net primary productivity, leaf area index, biome

Based on our reconstructions of minimum and maximum annual temperature, and monthly temperature and precipitation, we derived 17 bioclimatic variables [17] listed in Table 1. In addition, we used the Biome4 global vegetation model [10] to compute net primary productivity, leaf area index and biome type at a 0.5° resolution for all $t \in T_{120k}$, using reconstructed minimum annual temperature, monthly temperature, precipitation and cloudiness. Since Biome4 estimates ice biomes only based on climatic conditions and not ice sheet data, it can underestimate the spatial extent of ice. We therefore changed simulated non-ice biomes to ice in grid cells covered by ice sheets according to the ICE-6g dataset [19] at the relevant points in time.

Data Records

Our dataset, containing the variables listed in Table 1, is available as a single NetCDF file on **TBA**. All maps are provided at 2,000 year time steps between 120,000 BP and 22,000 BP, and 1,000 year time steps between 22,000 BP and the present. We used a 0.5° equirectangular grid, with longitudes ranging between 179.75°E and 179.75°W, and latitudes ranging between 59.75°S and 89.75°N. Non-land grid points are set to missing values, all other data are provided as 32-bit single precision floating point numbers.

Technical Validation

Our data show a good agreement with empirical reconstructions of mean annual temperature, temperature of the coldest and warmest month, and annual precipitation available for the mid-Holocene and the Last Glacial Maximum [2], and reconstructions of mean annual temperature available for the Last Interglacial Period [24] (Fig. 2, Fig. 3). The performance is well within the range of that of downscaled and bias-corrected outputs from other climate models available for specific points in the past (Fig. 3). By construction of the Delta Method, our present-day data is identical to the empirically observed climate.

Simulated vegetation, a product of monthly temperature, precipitation and cloud cover data, also corresponds well to mid-Holocene and Last Glacial Maximum empirical biome reconstructions [8] (Fig. 2).

Code availability

Code used to generate our dataset is available on **TBA**.

Acknowledgements

R.M.B., M.K. and A.M. were supported by ERC Consolidator Grant 647797 LocalAdaptation. We would like to thank Paul Valdes for his support with the HadCM3 and HadAM3H climate data.

Author contributions

R.M.B. developed and implemented the methods, generated the dataset, and wrote the manuscript.
M.K. developed the methods, prepared the climate model outputs, and revised the manuscript.
A.M. developed the methods and revised the manuscript.

Competing interests

The authors declare no competing interests.

Figures

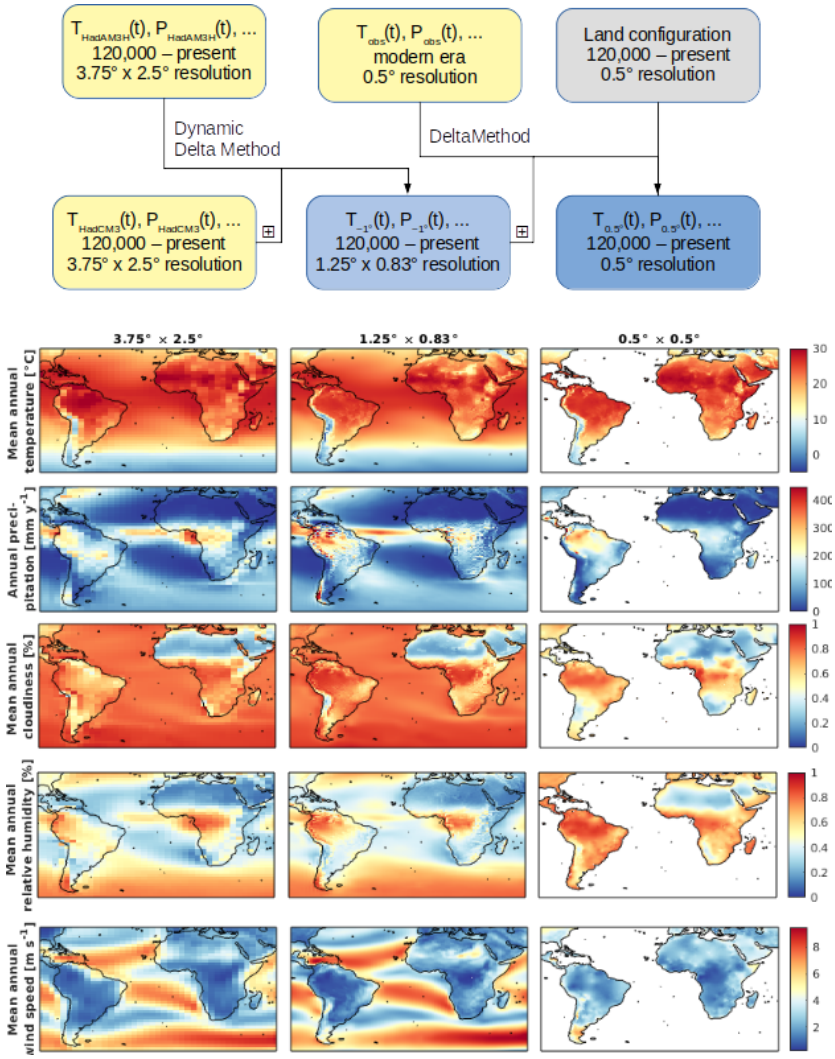

Figure 1: Reconstructing high-resolution climate. Yellow boxes represent raw simulated and observed data, the dark blue box represents the final data. Maps, showing present-day climate, correspond to the datasets represented by the bottom three boxes.

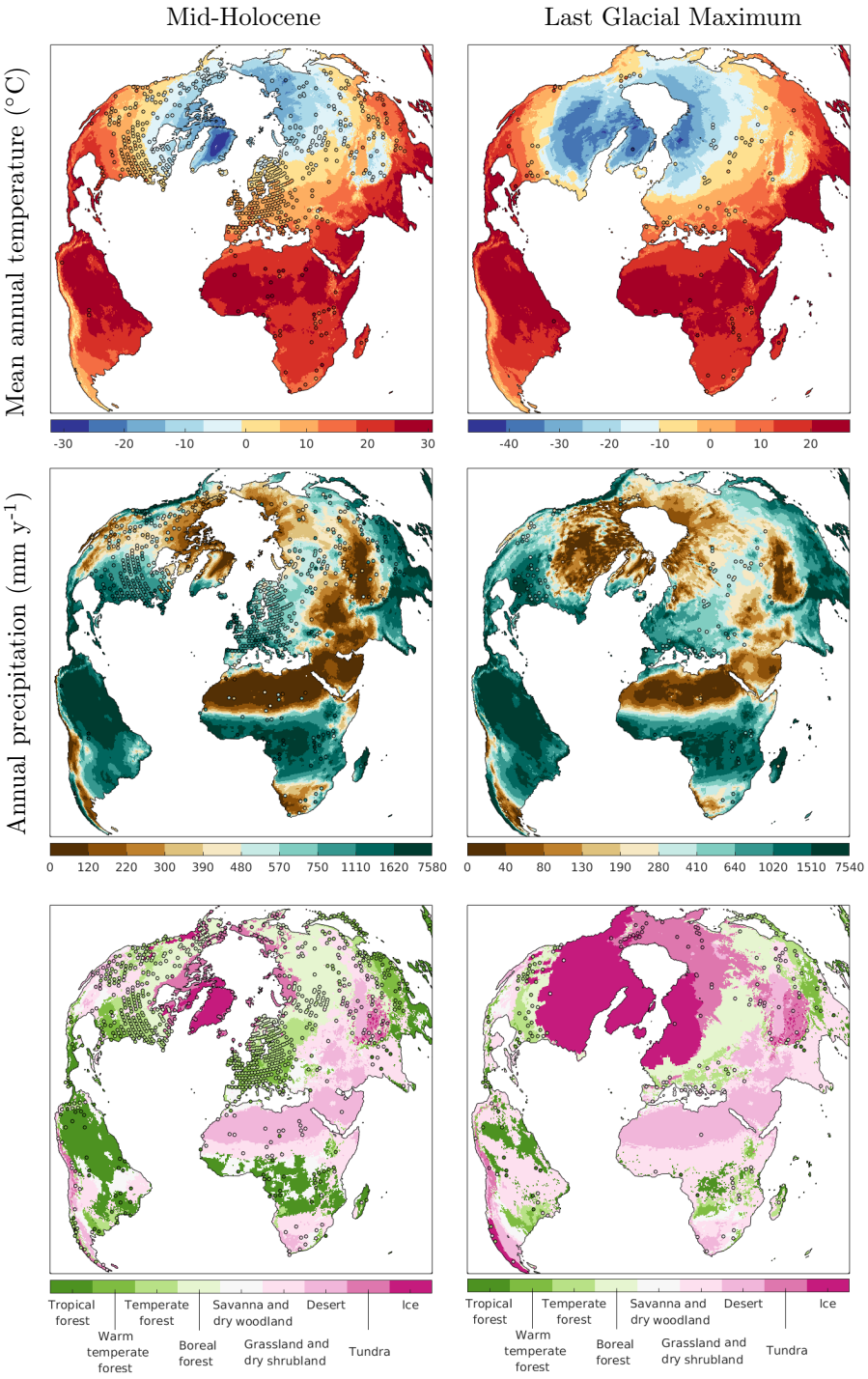

Figure 2: Comparison between modelled mid-Holocene and Last Glacial Maximum temperature, precipitation and vegetation (maps), and pollen-based empirical reconstructions (markers; uncertainties not shown). For visualisation purposes, empirical biomes were aggregated to a 2° grid, and the set of 27 simulated biomes was grouped into 9 megabiomes.

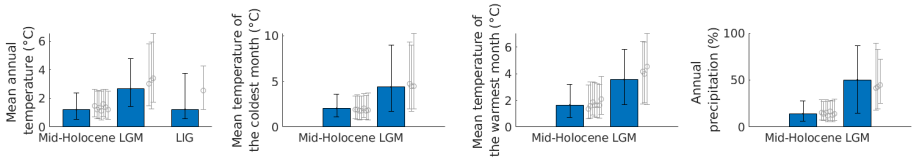

Figure 3: Quantitative comparison between our data to empirical reconstructions and other available model data. Bars and error bars represent the median and the upper and lower quantiles of the set of absolute differences between simulated and empirical data in locations where empirical reconstructions are available (cf. [3] for details). Grey error bars show the same measures for palaeoclimate data available on WorldClim [9], i.e. from the IPSL-CM5A-LR, MRI-CGCM3, BCC-CSM1-1, CNRM-CM5 and CCSM4 models (Mid-Holocene), the MPI-ESM-P and MIROC-ESM models (Mid-Holocene and Last Glacial Maximum) and the CCSM4 model (Last Glacial Maximum and Last Interglacial Period).

Tables

Variable	Unit	Dimensions
Dimensional variables		
Longitude	degrees east	720
Latitude	degrees north	300
Month	–	12
Year	before present	72
Climatic variables		
Monthly temperature	°C	720×300×12×72
Monthly precipitation	mm $month^{-1}$	720×300×12×72
Monthly cloudiness	%	720×300×12×72
Minimum annual temperature	°C	720×300×72
Maximum annual temperature	°C	720×300×72
Relative humidity	%	720×300×72
Wind speed	m $second^{-1}$	720×300×72
Bioclimatic variables		
BIO1: Annual mean temperature	°C	720×300×72
BIO4: Temperature seasonality	°C	720×300×72
BIO5: Minimum annual temperature	°C	720×300×72
BIO6: Maximum annual temperature	°C	720×300×72
BIO7: Temperature annual range	°C	720×300×72
BIO8: Mean temperature of the wettest quarter	°C	720×300×72
BIO9: Mean temperature of driest quarter	°C	720×300×72
BIO10: Mean temperature of warmest quarter	°C	720×300×72
BIO11: Mean temperature of coldest quarter	°C	720×300×72
BIO12: Annual precipitation	mm $year^{-1}$	720×300×72
BIO13: Precipitation of wettest month	mm $month^{-1}$	720×300×72
BIO14: Precipitation of driest month	mm $month^{-1}$	720×300×72
BIO15: Precipitation seasonality	–	720×300×72
BIO16: Precipitation of wettest quarter	mm $quarter^{-1}$	720×300×72
BIO17: Precipitation of driest quarter	mm $quarter^{-1}$	720×300×72
BIO18: Precipitation of warmest quarter	mm $quarter^{-1}$	720×300×72
BIO19: Precipitation of coldest quarter	mm $quarter^{-1}$	720×300×72
Vegetation variables		
Net primary productivity	gC m^{-2} $year^{-1}$	720×300×72
Leaf area index	gC m^{-2}	720×300×72
Biome	categorial	720×300×72

Table 1: Available reconstructions of environmental variables. Temperature seasonality (BIO4) and precipitation seasonality (BIO15) are given by the standard deviation of monthly temperatures and by the coefficient of variation of monthly precipitation, respectively. Temperature annual range (BIO7) is given by the difference between maximum annual temperature (BIO5) and minimum annual temperature (BIO6). Unit abbreviations: mm (millimetres), m (metres), gC (grams carbon).

References

[1] Hiroshi Akima. A new method of interpolation and smooth curve fitting based on local procedures. *Journal of the ACM (JACM)*, 17(4):589–602, 1970.

[2] PJ Bartlein, SP Harrison, Sandra Brewer, S Connor, BAS Davis, K Gajewski, Joel Guiot, TI Harrison-Prentice, A Henderson, Odile Peyron, et al. Pollen-based continental climate reconstructions at 6 and 21 ka: a global synthesis. *Climate Dynamics*, 37(3-4):775–802, 2011.

[3] Robert Beyer, Mario Krapp, and Andrea Manica. A systematic comparison of bias correction methods for paleoclimate simulations. *Climate of the Past Discussion*, DOI: 10.5194/cp-2019-11, 2019.

[4] Jason L Brown, Daniel J Hill, Aisling M Dolan, Ana C Carnaval, and Alan M Haywood. Paleoclim, high spatial resolution paleoclimate surfaces for global land areas. *Scientific data*, 5:180254, 2018.

[5] National Geophysical Data Center. 5-minute gridded global relief data (etopo5), 1993.

[6] Anders Eriksson, Lia Betti, Andrew D Friend, Stephen J Lycett, Joy S Singarayer, Noreen von Cramon-Taubadel, Paul J Valdes, Francois Balloux, and Andrea Manica. Late pleistocene climate change and the global expansion of anatomically modern humans. *Proceedings of the National Academy of Sciences*, 109(40):16089–16094, 2012.

[7] IPDJ Harris, Philip D Jones, Timothy J Osborn, and David H Lister. Updated high-resolution grids of monthly climatic observations–the cru ts3. 10 dataset. *International journal of climatology*, 34(3):623–642, 2014.

[8] Sandy Harrison. Biome 6000 db classified plotfile version 1, 2017.

[9] Robert J Hijmans, Susan E Cameron, Juan L Parra, Peter G Jones, and Andy Jarvis. Very high resolution interpolated climate surfaces for global land areas. *International journal of climatology*, 25(15):1965–1978, 2005.

[10] Jed O Kaplan, Nancy H Bigelow, I Colin Prentice, Sandy P Harrison, Patrick J Bartlein, Torben R Christensen, Wolfgang Cramer, Nadya V Matveyeva, A David McGuire, David F Murray, et al. Climate change and arctic ecosystems: 2. modeling, paleodata-model comparisons, and future projections. *Journal of Geophysical Research: Atmospheres*, 108(D19), 2003.

[11] Mario Krapp, Robert Beyer, Stephen L Edmundson, Paul J Valdes, and Andrea Manica. A comprehensive climate history of the last 800 thousand years. 2019.

[12] Matheus Souza Lima-Ribeiro, Sara Varela, Javier González-Hernández, Guilherme de Oliveira, José Alexandre F Diniz-Filho, and Levi Carina Terribile. Ecoclimate: a database of climate data from multiple models for past, present, and future for macroecologists and biogeographers. *Biodiversity Informatics*, 10, 2015.

[13] Eline D Lorenzen, David Nogués-Bravo, Ludovic Orlando, Jaco Weinstock, Jonas Binladen, Katharine A Marske, Andrew Ugan, Michael K Borregaard, M Thomas P Gilbert, Rasmus Nielsen, et al. Species-specific responses of late quaternary megafauna to climate and humans. *Nature*, 479(7373):359, 2011.

[14] Douglas Maraun and Martin Widmann. *Statistical downscaling and bias correction for climate research*. Cambridge University Press, 2018.

[15] Mark New, David Lister, Mike Hulme, and Ian Makin. A high-resolution data set of surface climate over global land areas. *Climate research*, 21(1):1–25, 2002.

[16] David Nogués-Bravo. Predicting the past distribution of species climatic niches. *Global Ecology and Biogeography*, 18(5):521–531, 2009.

[17] Michael S O'Donnell and Drew A Ignizio. Bioclimatic predictors for supporting ecological applications in the conterminous united states. *US Geological Survey Data Series*, 691(10), 2012.

[18] Richard G Pearson and Terence P Dawson. Predicting the impacts of climate change on the distribution of species: are bioclimate envelope models useful? *Global ecology and biogeography*, 12(5):361–371, 2003.

[19] WR Peltier, DF Argus, and R Drummond. Space geodesy constrains ice age terminal deglaciation: The global ice-6g_c (vm5a) model. *Journal of Geophysical Research: Solid Earth*, 120(1):450–487, 2015.

[20] Joy S Singarayer and Paul J Valdes. High-latitude climate sensitivity to ice-sheet forcing over the last 120 kyr. *Quaternary Science Reviews*, 29(1-2):43–55, 2010.

[21] Rachel M Spratt and Lorraine E Lisiecki. A late pleistocene sea level stack. *Climate of the Past*, 12(4):1079–1092, 2016.

[22] Jens-Christian Svenning, Camilla Fløjgaard, Katharine A Marske, David Nógues-Bravo, and Signe Normand. Applications of species distribution modeling to paleobiology. *Quaternary Science Reviews*, 30(21-22):2930–2947, 2011.

[23] Axel Timmermann and Tobias Friedrich. Late pleistocene climate drivers of early human migration. *Nature*, 538(7623):92, 2016.

[24] Chris SM Turney and Richard T Jones. Does the agulhas current amplify global temperatures during super-interglacials? *Journal of Quaternary Science*, 25(6):839–843, 2010.

[25] Paul J Valdes, Edaward Armstrong, Marcus PS Badger, Catherine D Bradshaw, Fran Bragg, Taraka Davies-Barnard, Jonathan J Day, Alex Farnsworth, Peter O Hopcroft, Alan T Kennedy, et al. The bridge hadcm3 family of climate models: Hadcm3@ bristol v1. 0. *Geoscientific Model Development*, 10:3715–3743, 2017.